BIOCHEMISTRY
including biophysical chemistry & molecular biology

Article

pubs.acs.org/biochemistry

Synergistic Effect of Pb^{2+} and Phosphatidylinositol 4,5-Bisphosphate on C2 Domain–Membrane Interactions

Krystal A. Morales and Tatyana I. Igumenova*

Department of Biochemistry and Biophysics, Texas A&M University, 300 Olsen Boulevard, College Station, Texas 77843-2128, United States

Supporting Information

ABSTRACT: Ca^{2+}-responsive C2 domains are peripheral membrane modules that target their host proteins to anionic membranes upon binding Ca^{2+} ions. Several C2 domain-containing proteins, such as protein kinase C isoenzymes (PKCs), have been identified as molecular targets of Pb^{2+}, a known environmental toxin. We demonstrated previously that the C2 domain from PKCα (C2α) binds Pb^{2+} with high affinity and undergoes membrane insertion in the Pb^{2+}-complexed form. The objective of this work was to determine the effect of phosphatidylinositol 4,5-bisphosphate (PIP_2) on the C2α–Pb^{2+} interactions. Using nuclear magnetic resonance (NMR) experiments, we show that Pb^{2+} and PIP_2 synergistically enhance each other's affinity for C2α. Moreover, the affinity of C2α for PIP_2 increases upon progressive saturation of the metal-binding sites. Combining the NMR data with the results of protein-to-membrane Förster resonance energy transfer and vesicle sedimentation experiments, we demonstrate that PIP_2 can influence two aspects of C2α–Pb^{2+}–membrane interactions: the affinity of C2α for Pb^{2+} and the association of Pb^{2+} with the anionic sites on the membrane. Both factors may contribute to the toxic effect of Pb^{2+} resulting from the aberrant modulation of PKCα activity. Finally, we propose a mechanism for Pb^{2+} outcompeting Ca^{2+} from membrane-bound C2α.

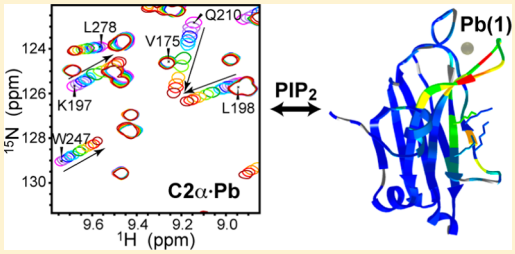

Conserved homology 2 (C2) domains are found in ~100 known eukaryotic host proteins that play key roles in signal transduction and membrane trafficking.[1] C2 domains, many of which function as Ca^{2+} sensors within their host proteins, are independently folded structural and functional modules of ~130 amino acids.[2−4] The binding of two or more Ca^{2+} ions[5−8] drives the association of Ca^{2+}-responsive C2 domains with lipid membranes, where they recognize the headgroup of phosphatidylserine (PtdSer) and other anionic phospholipids.[8−12] The role of metal ions in promoting C2–membrane association was proposed to be threefold:[1] (i) modulation of the C2 electrostatic potential,[13,14] (ii) direct coordination of the anionic lipid headgroup(s),[15] and (iii) facilitation of the interdomain rearrangement in multidomain proteins.[16,17]

C2 domains can interact with Pb^{2+}, a potent environmental toxin that acts as a Ca^{2+} surrogate in the context of specific molecular targets.[18] Interaction of Pb^{2+} with several Ca^{2+}-dependent C2 domain-containing proteins has been implicated in the disruption of neurotransmitter release,[19] which is a hallmark of Pb^{2+} poisoning. One of the notable examples is synaptotagmin 1, a membrane-associated Ca^{2+} sensor protein that is localized to the synaptic vesicles. The Ca^{2+} sensing function of synaptotagmin 1 is conducted by two C-terminal C2 domains: C2A and C2B. Pb^{2+} was found to be ~1000-fold more potent than Ca^{2+} in driving the association of synaptotagmin 1 with lipid membranes; in addition, Pb^{2+} ions disrupted the interactions between synaptotagmin 1 and its molecular partner, syntaxin.[20]

Another example is conventional protein kinase C isoenzymes (cPKCs) that comprise α, βI/βII, and γ isoforms.[21,22] The stimulatory effect of PKCs on neurotransmitter release has been attributed to the phosphorylation of ion channels and neuronal proteins involved in synaptic vesicle dynamics.[23] It has also been demonstrated that activation of PKC increases the size of the readily releasable vesicle pool and the rate at which it is replenished.[24] The kinase function of cPKCs is activated upon translocation of the protein to the plasma membrane in response to binding two second messengers: Ca^{2+} and diacylglycerol. A single C2 domain is responsible for the Ca^{2+}-induced activation of cPKCs. Following the original report of Pb^{2+} modulating cPKC activity,[25] a number of studies demonstrated that conventional cPKCs are activated by picomolar-to-nanomolar and partially inhibited by micromolar concentrations of Pb^{2+}.[26−28] Experiments with the recombinant PKCα isoform provided evidence of the existence of three Pb^{2+} interaction sites.[28] Recently, our laboratory reported that the high-affinity Pb^{2+} interaction site resides on the C2 domain of PKCα.[6]

Despite the well-documented effect of Pb^{2+} on the membrane-dependent activity of C2 domain-containing proteins, the molecular mechanism of the action of Pb^{2+} at the membrane is not fully understood. The objective of this

Received: December 15, 2011
Revised: February 28, 2012
Published: April 4, 2012

work was to determine the influence of a lipid second messenger, phosphatidylinositol 4,5-bisphosphate (PIP_2), on the interactions of C2 domains with Pb^{2+}.

PIP_2 is involved in the regulation of a variety of cellular processes,[29,30] including synaptic vesicle trafficking.[31] PIP_2 is selectively enriched in the cytoplasmic leaflet of the plasma membrane, where it occurs at a molar concentration of 1−3%. The significance of PIP_2 as a modulator of C2 domain−membrane interactions became apparent upon detection of its specific binding to the C2 domains from conventional PKC isoforms,[32,33] synaptotagmin 1,[34,35] and rabphilin-3A.[36,37] The presence of PIP_2 in PtdSer-containing lipid membranes increases the affinity of Ca^{2+} for C2 domains[33,38−40] and makes them responsive to Ca^{2+} concentrations that are typically associated with the Ca^{2+} spike during signaling. The role of PIP_2 as a sole determinant of localization of PKCα to the plasma membrane is still being debated.[38,41] However, there is general agreement that the presence of PIP_2 in the membrane results in a decrease in the C2α off rate and, as a result, the increased residency time of the protein on the plasma membrane.[38,39]

To determine the influence of PIP_2 on C2−Pb^{2+} interactions, we used the C2 domain from PKCα (C2α) as a paradigm for Ca^{2+}-responsive C2 domains. In one of the first studies of the C2α−PIP_2 system, Corbalán-García et al.[32] demonstrated that C2α could bind to membrane-embedded PIP_2 even in the absence of the PtdSer component, albeit with a lower affinity. Another unexpected finding was that the association of C2α and PIP_2 occurred even in the absence of Ca^{2+}. The specific region of C2α involved in PIP_2 interactions, which is distinct from the PtdSer-binding site, was identified using mutagenesis.[32,42] A subsequent determination of the crystal structure of the ternary C2α−Ca^{2+}−PIP_2 complex revealed the molecular details of the PIP_2 site.[43] Figure 1 shows the structure of the

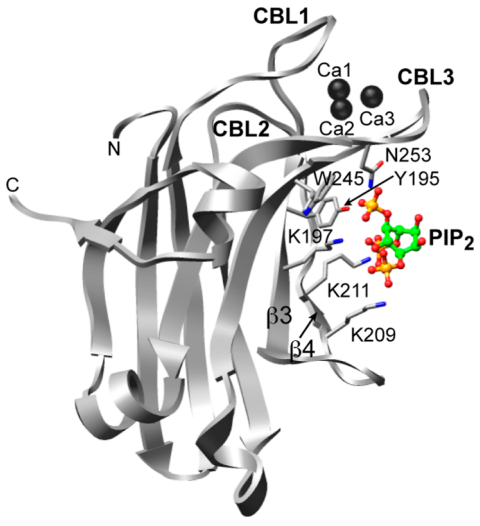

Figure 1. Structure of the C2α−Ca^{2+}−PIP_2 complex (Protein Data Bank entry 3GPE)[43] showing the details of the PIP_2 interaction site. CBL1−CBL3 are the Ca^{2+}-binding loops.

complex with all functional regions highlighted. The tip of the C2α domain comprises three calcium-binding loops (CBLs). Two of them, CBL1 and CBL3, coordinate calcium ions. Electron paramagnetic resonance studies identified CBL1 and CBL3 as the protein segments that penetrate the lipid headgroup region of the PtdSer-containing membranes.[44] The PIP_2-binding site is mostly formed by two β-strands, β3 and β4. A total of six residues are involved in the interactions with the oxygen atoms of the three phosphate groups in PIP_2: Y195, K197, K209, K211, W245, and N253. The three lysines that belong to strands β3 and β4 (K197, K209, and K211) are part of the region that has been termed in the literature the "β-groove", "polybasic cluster", or "lysine-rich cluster". We will use the term lysine-rich cluster in this paper.

Recently, our laboratory has characterized the interactions of C2α with Pb^{2+} in the presence and absence of PtdSer-containing model membranes.[6] We determined the crystal structure of Pb^{2+}-complexed C2α, established that C2α has two Pb^{2+}-binding sites with a 2000-fold difference in binding affinities, and demonstrated that Pb^{2+} can outcompete Ca^{2+} from C2α in the presence of PtdSer-containing model membranes. In this work, we employed nuclear magnetic resonance (NMR) spectroscopy, protein-to-membrane Förster resonance energy transfer (FRET), and vesicle sedimentation experiments to determine the effect of PIP_2 on the C2α−Pb^{2+} and C2α−Pb^{2+}−membrane interactions. Our findings not only shed light on the molecular mechanism of C2α−Pb^{2+}−PIP_2 interactions but also illustrate the contribution of PIP_2 to Pb^{2+} interfering with the Ca^{2+}-dependent function of C2α.

EXPERIMENTAL PROCEDURES

Materials. 1-palmitoyl-2-oleoyl-*sn*-glycero-3-phosphocholine (POPC), 1-palmitoyl-2-oleoyl-*sn*-glycero-3-phospho-L-serine (POPS), L-α-phosphatidylinositol 4,5-bisphosphate (brain, porcine) (bp-PIP_2), and 1,2-dioleoyl-*sn*-glycero-3-phosphoethanolamine-*N*-(5-dimethylamino-1-naphthalenesulfonyl) (dansyl-PE) were obtained from Avanti Polar Lipids Inc. (Alabaster, AL). Short chain (C4) D-myophosphatidylinositol 4,5-bisphosphate (C4-PIP_2) used for NMR-detected titrations was purchased from Echelon Bioscience (Salt Lake City, UT). The ion-chelating resin, Chelex 100 (Sigma-Aldrich), was used to treat all buffers to remove residual divalent metal ions.

Overexpression and Purification of C2α. Overexpression and purification of C2α were conducted as previously described.[6] Uniformly ^{15}N-enriched ([U-^{15}N]) C2α was prepared using the method of Marley et al.[45] Decalcification of C2α was accomplished by conducting the last purification step in the presence of 0.1 mM ethylenediaminetetraacetic acid (EDTA). EDTA was subsequently removed by several rounds of solvent exchange into a decalcified 10 mM MES buffer (pH 6.0) and 100 mM KCl.

Binding of C4-PIP_2 to C2α Monitored by NMR. The binding of C4-PIP_2 to [U-^{15}N]C2α was monitored using NMR-detected titration experiments. All experiments were conducted at 25 °C on a Varian Inova spectrometer operating at a ^1H Larmor frequency of 600 MHz (14.1 T). A series of ^{15}N−^1H heteronuclear single-quantum coherence (HSQC) spectra were collected for C2α in three different states of metal ligation, apo, Ca^{2+}-bound, and single Pb^{2+}-bound, at increasing concentrations of C4-PIP_2.

The Ca^{2+}-bound state, C2α·Ca_2, was prepared by adding Ca^{2+} to a final concentration of 2.5 mM to 100 μM apo C2α. The single Pb^{2+}-bound C2α, C2α·Pb, was prepared by adding Pb^{2+} to a final concentration of 100 μM to 100 μM apo-C2α. We observed significant precipitation of C4-PIP_2 at Pb^{2+} concentrations that are required to generate the C2α·Pb_2 state. This prevented us from conducting the C4-PIP_2 titration experiments on the C2α·Pb_2 complex. To determine the affinity of Pb^{2+} for the second C2α site in the presence of a saturating

dx.doi.org/10.1021/bi201850h | *Biochemistry* 2012, 51, 3349−3360

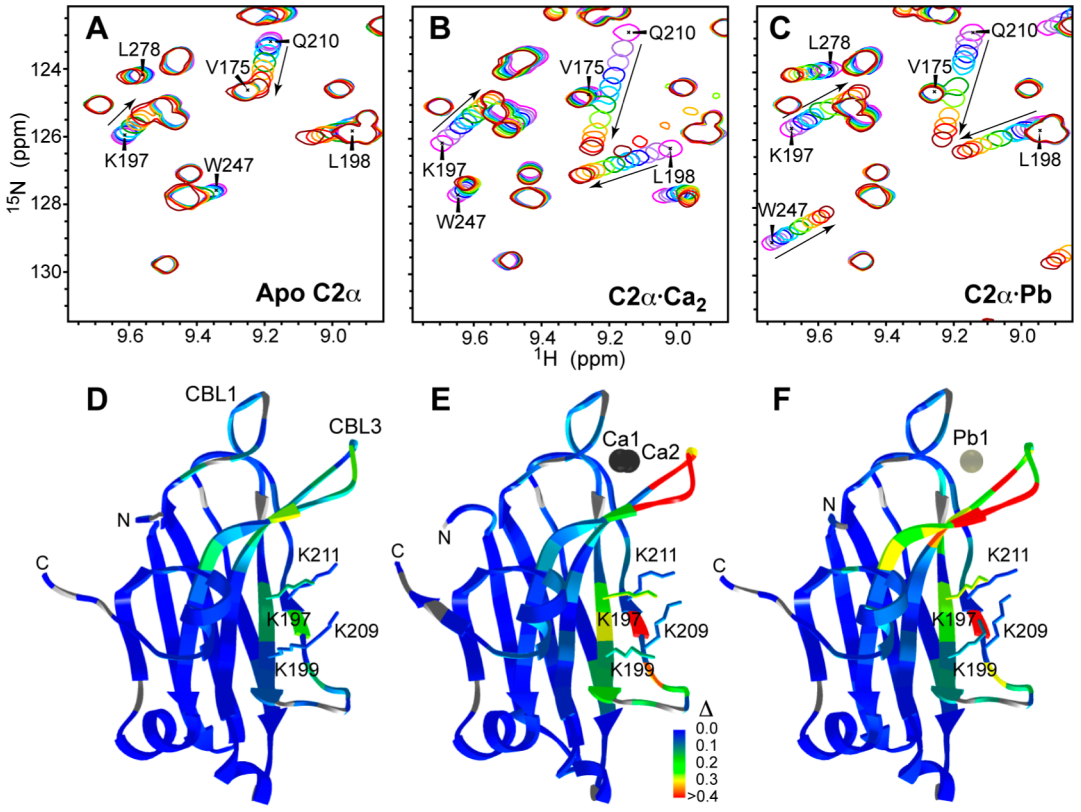

Figure 2. Expansions of $^{15}N-^{1}H$ HSQC spectra of 100 μM apo C2α (A), C2α·Ca_2 (B), and C2α·Pb (C) at different concentrations of C4-PIP_2. The arrows point in the direction of increasing C4-PIP_2 concentration, which varies from 0 to 1.5 mM for apo-C2α and C2α·Pb and from 0 to 1 mM for C2α·Ca_2. Site-specific Δ values were calculated according to eq 1, color-coded, and mapped onto the structures of apo (D), Ca^{2+}-complexed (E), and Pb^{2+}-complexed (F) C2α. The side chains of K197, K199, K209, and K211 indicate the position of the lysine-rich cluster. Prolines and N-terminal residue T156, for which NMR data are not available, are colored gray.

level of C4-PIP_2, we titrated Pb^{2+} into the preformed C2α·Pb·PIP_2 complex. The concentration of C4-PIP_2 in the mixture was 1.5 mM. The NMR buffer for all experiments consisted of 10 mM MES (pH 6.0), 100 mM KCl, 8% D_2O, and 0.02% NaN_3. The C4-PIP_2 stock solution was standardized using a phosphate quantification assay.[46] NMR data were processed with NMRPipe[47] and analyzed using Sparky.[48]

Site-specific chemical shift perturbations of C2α due to ligand binding were calculated according to the following equation:

$$\Delta = [\Delta\delta_H{}^2 + (0.152\Delta\delta_N)^2]^{1/2} \quad (1)$$

where $\Delta\delta_H$ and $\Delta\delta_N$ are the residue-specific chemical shift changes between the two states that are being compared and 0.152 is the scaling factor.[49]

Binding curves were constructed by plotting the change in C2α chemical shift as a function of the total ligand concentration. The dissociation constants, K_d, were determined by globally fitting the binding curves with a single-site binding equation:[50]

$$\Delta\delta = (\Delta\delta_{PL}/2P_0)\{K_d + P_0 + L_0 - [(K_d + P_0 + L_0)^2 - 4P_0L_0]^{1/2}\} \quad (2)$$

where $\Delta\delta$ is a combined residue-specific change in chemical shift at total ligand concentration L_0, P_0 is the total protein concentration, and $\Delta\delta_{PL}$ is the residue-specific chemical shift difference between the complexed and free protein species.

Association of C2α with PIP_2-Containing Membranes Measured by FRET. Protein-to-membrane FRET experiments were conducted using the ISS Phoenix spectrofluorometer. The Trp residues of C2α and the dansyl-PE lipid component of the large unilamellar vesicles (LUVs) were used as the donor and acceptor, respectively. The LUVs consisted of POPC, POPS, bp-PIP_2, and dansyl-PE in a 61:30:2:7 molar ratio. Fluorescence emission spectra of the sample containing 0.5 μM C2α and LUVs (total lipid concentration of 150 μM) were collected at increasing concentrations of the metal ion, Ca^{2+} or Pb^{2+}. The spectra were corrected by subtracting the fluorescence of the reference sample that contained all components but C2α. The change in FRET intensity at 505 nm generated upon C2α membrane binding, ΔF, relative to the maximal attainable change, ΔF_{max}, was plotted as a function of the total metal concentration. Data were fit with the following equation:

$$\Delta F/\Delta F_{max} = \frac{[M^{2+}]^H}{[M^{2+}]^H + [M^{2+}]_{1/2}{}^H} \quad (3)$$

where H is the Hill coefficient and $[M^{2+}]_{1/2}$ is the metal concentration required for half-maximal binding.

Calculations of the Protein Electrostatic Potential. The calculations were conducted using the Adaptive Poisson–Boltzmann Solver (APBS)[51] implemented through the Visual Molecular Dynamics (VMD)[52] plugin. The Protein Data Bank (PDB) files were prepared for electrostatics calculations using PDB2PQR.[53] The parametrization of the PIP_2 ligand produced a net charge of −4, which is consistent with the available

dx.doi.org/10.1021/bi201850h | Biochemistry 2012, 51, 3349–3360

experimental evidence.[54] Pb^{2+} ions were parametrized with a Born radius of 2.17 Å.[55] Figures showing the surface-mapped electrostatic potential were generated with VMD.

RESULTS

C2α Binds PIP_2 in All Three States of Metal Ligation. To determine the effect of Pb^{2+} on the C2α–PIP_2 interactions, we conducted a series of NMR-detected titrations of C2α with a water-soluble C4-PIP_2. We made use of the single high-affinity Pb^{2+}-binding site on C2α and prepared the C2α·Pb state by mixing the equimolar quantities of protein and metal ion. To provide the reference for our Pb^{2+} data and determine the general role of divalent metal ions in modulating the affinity of C2α for PIP_2, we also tested the binding of C4-PIP_2 to the apo and Ca^{2+}-complexed forms of C2α. $^1H-^{15}N$ HSQC spectra were collected for [U-^{15}N]C2α that was prepared in three states of metal ligation, apo, Ca^{2+}-saturated (C2α·Ca_2), and a single Pb^{2+} bound (C2α·Pb), with C4-PIP_2 concentrations ranging from 0 to 1.5 mM.

The results are presented in Figure 2. Panels A–C are the expansions of the $^1H-^{15}N$ HSQC spectra that illustrate the response of the C2α N–H resonances (or cross-peaks) to increasing concentrations of C4-PIP_2. The amino acid identities of the C2α cross-peaks were determined previously using a set of triple-resonance NMR assignment experiments.[6] Full spectra are shown in Figure S1 of the Supporting Information. In all three states of metal ligation, the binding of C4-PIP_2 to C2α falls into the exchange regime that is fast on the NMR chemical shift time scale. In this regime, the cross-peak positions change smoothly as a result of increasing ligand concentrations. Based on the absolute value of chemical shift changes, Ca^{2+}- and Pb^{2+}-complexed forms of C2α show a more pronounced response to C4-PIP_2 binding than the apo form.

Chemical shift perturbations that are experienced by C2α residues between 0 and 1–1.5 mM C4-PIP_2 were calculated using eq 1. In all cases, we used the chemical shifts of the appropriate metal-ligated form as a reference state. Panels D–F of Figure 2 show the color-coded Δ values mapped onto the corresponding C2α crystal structures: apo (PDB entry 3RDJ),[6] Ca^{2+}-complexed (PDB entry 1DSY),[15] and Pb^{2+}-complexed (PDB entry 3TWY).[6] In the latter, only the Pb^{2+} ion that occupies the high-affinity C2α site is shown. The protein region affected by C4-PIP_2 binding is not limited to the lysine-rich cluster but also includes the calcium-binding loops.

This effect is further illustrated in Figure 3 by plotting the Δ values as a function of primary structure. Three C2α regions, irrespective of the metal-ligation state, experience chemical shift perturbation upon C4-PIP_2 binding: the lysine-rich cluster located on the β3–β4 segment; CBL1, which immediately precedes the β3–β4 region; and CBL3, which is distant from the β3–β4 region in the primary structure but is close to it in the tertiary structure. The weaker effect of PIP_2 binding on the apo state of C2α is evident from the magnitude of chemical shift perturbations. Given that the backbone conformation of the C2α–Ca^{2+}–PIP_2 complex is close to that of the apo form (the rmsd for the backbone atoms is 0.40 Å), the chemical shift perturbations are likely due to the changes in the electrostatic properties and/or conformational dynamics of the protein. The chemical shift perturbation pattern is very similar for C2α·Ca_2 and C2α·Pb (Figure 3B,C), indicating that a full complement of metal ions is not a stringent requirement for the C2α–PIP_2 interactions.

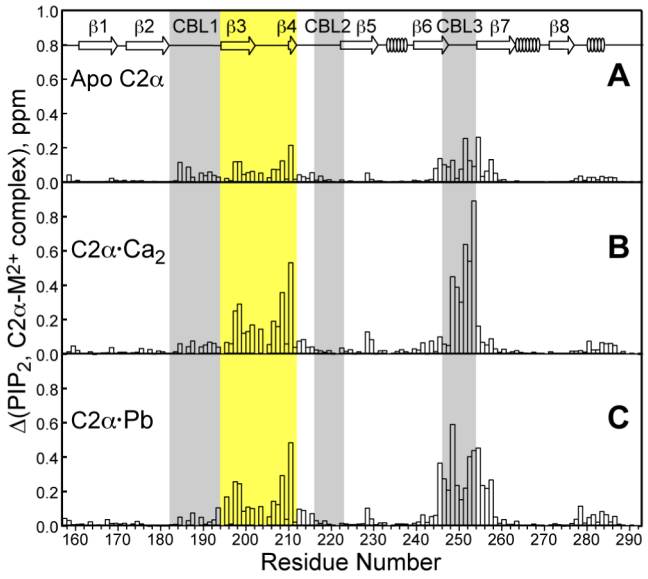

Figure 3. Chemical shift perturbation Δ due to PIP_2 binding plotted as a function of primary structure for apo C2α (A), C2α·Ca_2 (B), and C2α·Pb (C). Calcium-binding loops, CBL1 (residues 182–193), CBL2 (residues 216–222), and CBL3 (residues 246–253), are highlighted in gray. The β3–β4 region (residues 194–211) that directly interacts with PIP_2 is highlighted in yellow.

Pb^{2+} Enhances the Affinity of C2α for PIP_2. To obtain the affinities of C2α for C4-PIP_2, we constructed binding curves for all NH groups whose combined ^{15}N and ^1H chemical shift changed by more than 0.05 in the course of the titration. The data are presented in Figure 4 for two representative residues: K197 and Q210. Each panel in Figure 4 shows the residue-specific binding curves for three different states of metal ligation: apo C2α, C2α·Pb, and C2α·Ca_2.

In apo C2α, the binding curves for all but two PIP_2-responsive residues could be globally fit with eq 2, which yielded a K_d of 1130 ± 38 μM. These data indicate that, in the absence of metal ions and lipid membranes, C2α is a low-affinity PIP_2 binding module. Having a single Pb^{2+} bound to the high-affinity C2α site increases the affinity of the protein for PIP_2. The global fit of the C2α·Pb binding curves produced a K_d of 198 ± 2 μM. The C2α·Ca_2 state showed a more complex response to PIP_2. To facilitate the analysis of binding data, we separated the 38 responsive residues into three groups on the basis of their titration behavior. Group 1 comprises 27 members that either belong to the β3–β4 region or are in its immediate vicinity. Group 1 data can be well fit with the single-site binding equation to produce a K_d of 48 ± 1 μM (Figure 4). Groups 2 and 3 are further described in section entitled "Interplay between Ca2+ and PIP2".

In summary, the affinity of metal ion-complexed C2α for PIP_2 is significantly enhanced compared to that of the apo form. The K_d for the C2α·Pb·PIP_2 complex falls between the K_d values of the C2α·PIP_2 and C2α·Ca_2·PIP_2 complexes. This effect, the 4–6-fold decrease in K_d upon progressive saturation of C2α metal-binding sites, appears to depend mostly on the number of bound metal ions (and hence the overall charge of the protein).

Figure 5 highlights the contributions of individual metal-binding sites of C2α to PIP_2 binding. For this analysis, we chose the substoichiometric concentration of C4-PIP_2, 80 μM, to prevent the saturation regime, where the effect of the increased

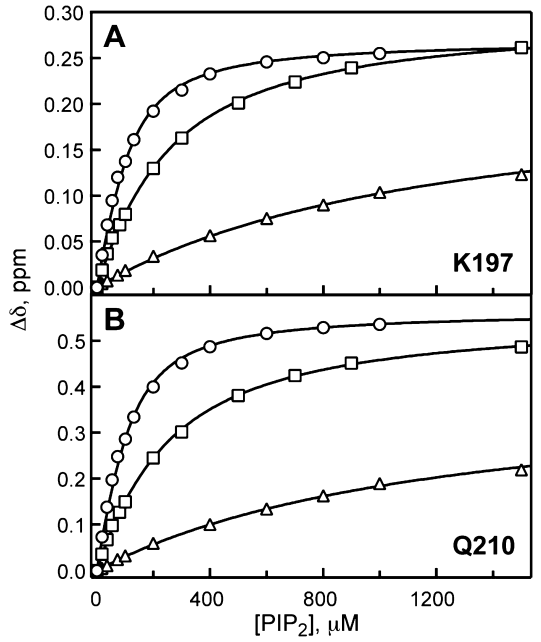

C2 state	K_d (μM)	# Residues used for fit
△ Apo C2α	1130 ± 38	16
□ C2α·Pb	198 ± 2	35
○ C2α·Ca_2	48 ± 1	27

Figure 4. C4-PIP_2 binding curves for K197 (A) and Q210 (B) in apo-C2α (△), C2α·Ca_2 (○), and C2α·Pb (□). Solid lines represent the fits to eq 2. $\Delta\delta$ is the absolute value of the chemical shift change in parts per million. The table summarizes the PIP_2 dissociation constants determined for three states of metal ligation.

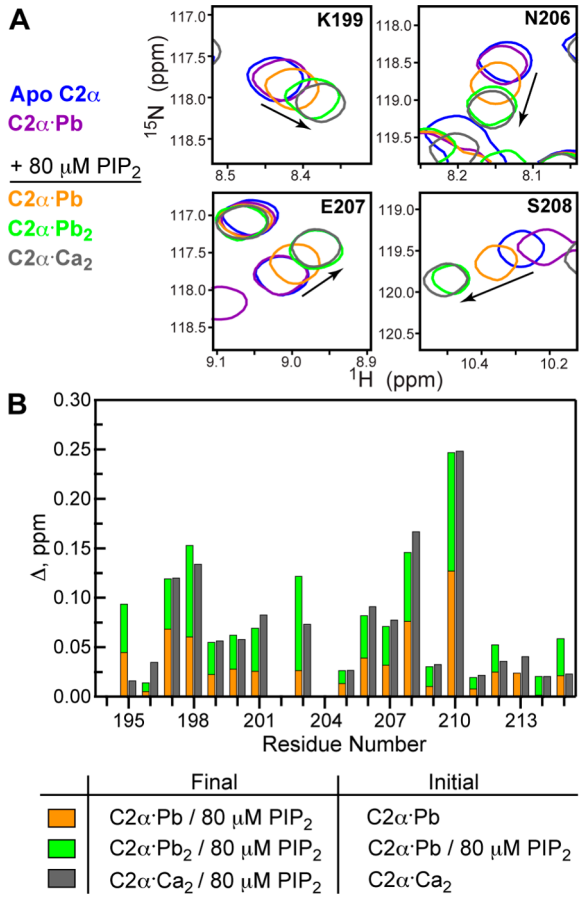

Figure 5. Individual contributions of C2α metal sites to PIP_2 binding. (A) Expansions of the $^{15}H-^{1}N$ HSQC spectra for four C2α residues from the $\beta3-\beta4$ region. (B) Chemical shift perturbations (Δ) for the $\beta3-\beta4$ region. Δ values were calculated according to eq 1 using the final and initial states listed in the table.

PIP_2 affinity would not be discernible. The residues chosen for the chemical shift perturbation analysis belong to the $\beta3-\beta4$ region. The residues from this region respond weakly if at all to metal ions but show significant perturbations in response to PIP_2 binding, as illustrated in Figure 5A (blue, purple, and orange spectra). The binding of the second Pb^{2+} ion to C2α results in the shift of cross-peaks that is solely due to the enhancement of the C2α affinity for PIP_2 (green spectrum). The spectra of Pb^{2+}-complexed (green) and Ca^{2+}-complexed (gray) C2α in the presence of 80 μM PIP_2 are virtually identical for the $\beta3-\beta4$ region, which is not the case for the CBLs.

The results of the chemical shift perturbation analysis are shown in Figure 5B. For the Pb^{2+} data, there are two processes that contribute to the observed C2α chemical shift change: the binding of PIP_2 to the C2α·Pb state (orange bars) and the binding of additional PIP_2 upon filling the second Pb^{2+}-binding site (green bars). For many residues in the $\beta3-\beta4$ region, the sum of these two contributions is virtually identical to the Δ values obtained for the binding of PIP_2 to the C2α·Ca_2 state (gray bars). This "additive" behavior illustrates that the enhancement of the C2α affinity for PIP_2 caused by metal ions does not depend on the identity of the metal ions, at least for the Ca^{2+} and Pb^{2+} pair.

PIP_2 Enhances the Affinity of C2α for Pb^{2+}. The next step was to determine the binding affinities of C2α for Pb^{2+} in the presence of a saturating level of PIP_2. The Pb^{2+} affinities of two C2α metal-binding sites, (1) and (2), differ 2000-fold. The K_d for high-affinity site (1) was determined in our previous study by isothermal titration calorimetry (ITC).[6] However, the quantities of C4-PIP_2 required to produce the PIP_2-saturated state of apo C2α make the ITC experiments cost-prohibitive in this case. Instead, we determined the K_d for low-affinity Pb^{2+} site (2) in the presence of a saturating level of PIP_2. This value, $K_{d2}^{Pb,PIP}$, was then used to calculate the dissociation constant for the first site, $K_{d1}^{Pb,PIP}$ (vide infra).

We prepared the C2α·Pb·PIP_2 complex by combining the equimolar amounts of C2α and Pb^{2+}, followed by the addition of C4-PIP_2 to a final concentration of 1.5 mM. According to the binding data of Figure 4, under these conditions, the C2α·Pb·PIP_2 complex is the dominant protein species in solution. The titration of the C2α·Pb·PIP_2 complex with Pb^{2+} was monitored using $^{15}N-^{1}H$ HSQC experiments. We identified the residues that responded to $Pb^{2+}(2)$ binding and constructed a total of eight binding curves. All of them were fit globally with eq 2, which produced a $K_{d2}^{Pb,PIP}$ of 17 ± 1 μM. An example of the binding curve for D248 is shown in Figure 6A. For comparison, on the same graph, we plotted the D248 data for $Pb^{2+}(2)$ binding to the C2α·Pb complex in the absence of PIP_2. The K_d for this process, 129 ± 4 μM, was determined in our previous work.[6] These data indicate that the prebound PIP_2 results in the 8-fold increase in the affinity of C2α for $Pb^{2+}(2)$.

To understand the effect of binding of $Pb^{2+}(2)$ on the PIP_2-complexed C2α, we conducted chemical shift perturbation analysis for the pair of PIP_2 complexes, C2α·Pb_2·PIP_2 and

dx.doi.org/10.1021/bi201850h | Biochemistry 2012, 51, 3349−3360

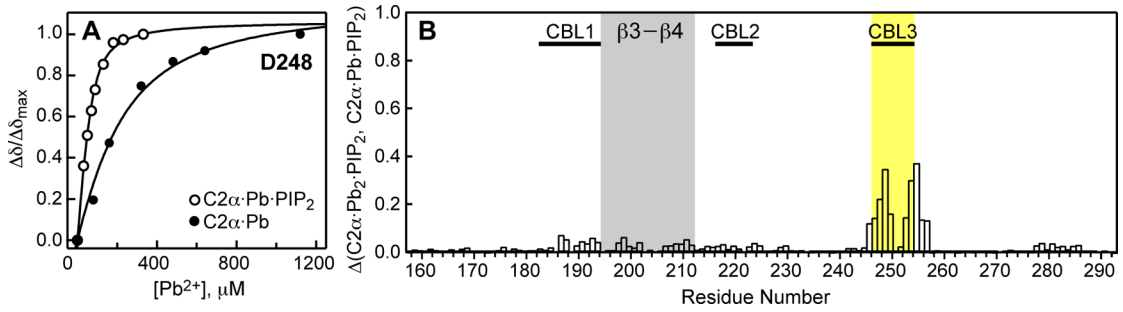

Figure 6. PIP_2 increases the affinity of C2α for Pb^{2+}(2). (A) D248 binding curves for the titration of C2α·Pb·PIP_2 (○) and C2α·Pb (●) complexes with Pb^{2+}(2). $\Delta\delta$ values are normalized to the maximal observed change, $\Delta\delta_{max}$. (B) Chemical shift perturbation analysis of the C2α·Pb_2·PIP_2 complex using the C2α·Pb·PIP_2 complex as a reference state. The β3-β4 and CBL3 regions are highlighted in gray and yellow, respectively.

C2α·Pb·PIP_2, with the latter used as a reference state. The results are shown in Figure 6B. It is evident that the binding of Pb^{2+}(2) to C2α mostly affects CBL3 and has little effect on CBL1 or the lysine-rich cluster.

Combining the data obtained in this work and previous work,[6] we constructed a full scheme of thermodynamic equilibria present in the C2α, Pb^{2+}, and PIP_2 system. We have experimentally determined the dissociation constants for five of seven binding equilibria, as indicated in Figure 7. Using

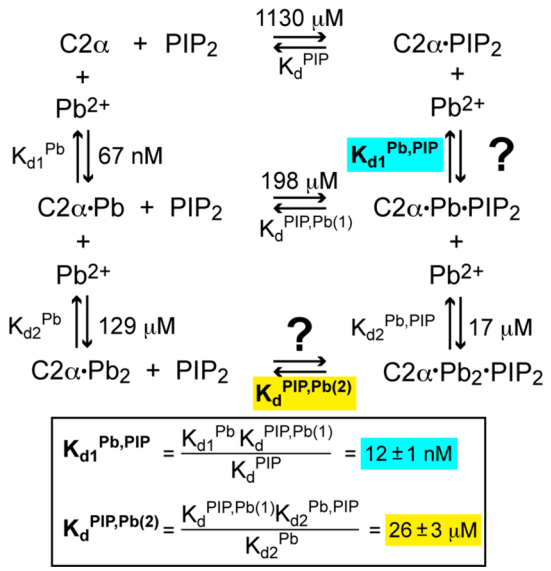

Figure 7. Thermodynamic binding equilibria and dissociation constants in the C2α, Pb^{2+}, and PIP_2 system. The constants calculated from the experimentally measured K_d values are highlighted for the Pb^{2+} (cyan) and PIP_2 (yellow) dissociation reactions.

simple thermodynamic considerations, we were able to calculate the two remaining dissociation constants. $K_{d1}^{Pb,PIP}$ for the dissociation of Pb^{2+}(1) from the C2α·Pb·PIP_2 complex is 12 nM; this represents an ~6-fold increase in the Pb^{2+}(1) affinity compared to that of the system lacking PIP_2. $K_d^{PIP,Pb(2)}$ for the dissociation of PIP_2 from the C2α·Pb_2·PIP_2 complex is 26 μM, which corresponds to an ~43-fold increase in PIP_2 affinity compared to that of apo C2α. In summary, our binding data clearly illustrate that Pb^{2+} and PIP_2 significantly enhance each other's interactions with C2α.

Interplay between Ca^{2+} and PIP_2. The NMR response of C2α·Ca_2 to PIP_2 binding was rather complex, which prompted us to separate the responsive residues into three groups. The 27 residues of group 1, the largest group, belong to the lysine-rich cluster and adjacent protein regions (vide supra). The residues of groups 2 and 3 could be fit with K_d values that are either above or below the K_d values that were obtained for the residues of group 1. The corresponding binding curves and the table of K_d values are given in Figure S2 of the Supporting Information. Panels A and B of Figure 8 show the NMR-detected binding curves for D248 and N253 as representative members of groups 2 and 3, respectively.

There are six residues in group 2: D248, T250, D254, F255, G257, and Q280. Four of them (D248, T250, D254, and F255) belong to CBL3 or its hinges, as shown in Figure 8C. Group 3 with five members (D187, G190, L191, Y195, and N253) maps onto the CBL1 region of C2α (Figure 8C, blue), with the exception of Y195 and N253, which reside on the β3 strand and CBL3, respectively.

There could be two possible explanations for the differences in the apparent PIP_2 dissociation constants. First, if the conformational dynamics of the PIP_2- and Ca^{2+}-complexed C2α is different from that of the Ca^{2+}-complexed C2α, this difference could contribute to the observed chemical shift changes during the PIP_2 titration. Second, an additional binding process that affects the backbone chemical shifts of specific protein segments and manifests itself as an apparent change in the affinity of C2α for PIP_2 could be present in the system. This additional process is likely to be the binding of the third Ca^{2+} ion to the PIP_2-complexed C2α. In the crystal structure of PIP_2-complexed C2α, Ca^{2+}(3) is coordinated by the carboxyl oxygens of D254 and D248, the side chain oxygen of T251, and the backbone carbonyl oxygen of R252. We know from our previous work that, in the absence of PIP_2, the Ca^{2+}(3) site is not populated under the conditions of our NMR experiments. However, the binding of PIP_2 to the C2α·Ca_2 complex may enhance the affinity of C2α for Ca^{2+}(3) in much the same way it enhances the affinity of the C2α·Pb·PIP_2 complex for Pb^{2+}(2) (vide supra). As a result, some protein residues may show the titration behavior that essentially reflects the two binding processes that involve PIP_2 and Ca^{2+}(3). As a final note, the heterogeneity in the apparent K_d values for group 2 and 3 residues is specific to the C2α·Ca^{2+} system where Ca^{2+} is in 25-fold excess with respect to protein and is not observed in the C2α·Pb complex, where there is no excess of metal ions.

A similar behavior with respect to PIP_2 binding was reported for another C2 domain, the C2A domain of rabphilin-3A.[37] Those data were interpreted as the existence of an additional, albeit weaker, PIP_2-binding site.

Pb^{2+} Promotes the Association of C2α with PIP_2-Containing Membranes. Our next step was to determine the

dx.doi.org/10.1021/bi201850h | Biochemistry 2012, 51, 3349−3360

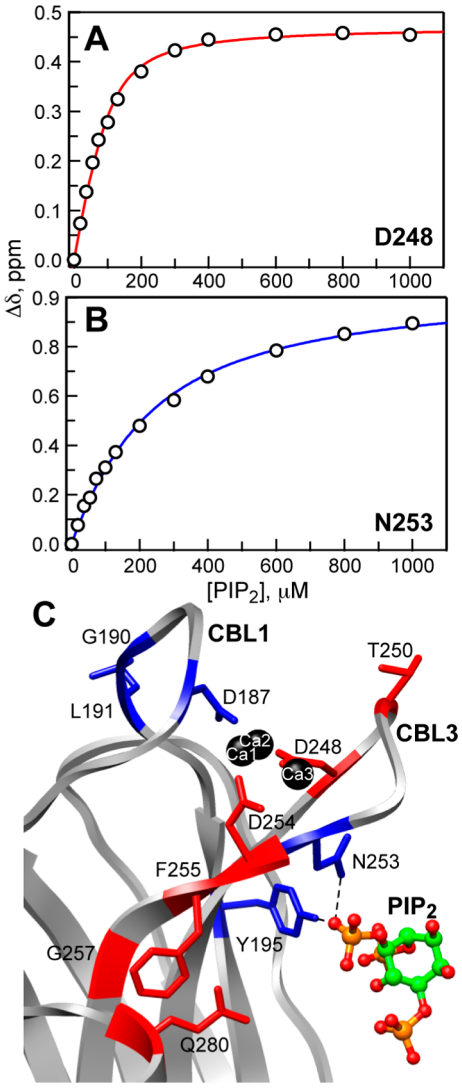

Figure 8. (A) NMR-detected PIP_2 binding curves for D248 from group 2 (K_d = 24 ± 1 μM) and N253 from group 3 (K_d = 175 ± 12 μM). (C) Group 2 (red) and group 3 (blue) residues mapped onto the crystal structure of Ca^{2+}- and PIP_2-complexed C2α (PDB entry 3GPE).

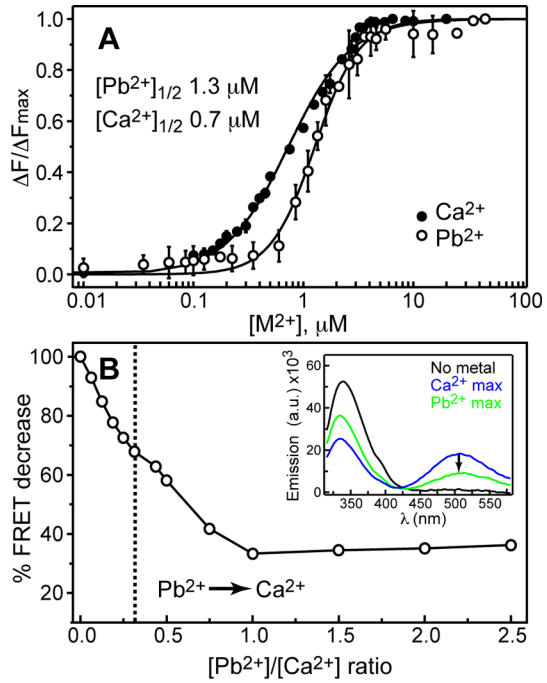

Figure 9. (A) Normalized protein-to-membrane FRET as a function of total Ca^{2+} and Pb^{2+} concentration in the presence of POPC/POPS/bp-PIP_2/dansyl-PE (61:30:2:7) LUVs. The error bars were calculated as standard deviations from triplicate experiments. (B) Decrease in FRET efficiency as a result of Ca^{2+} displacement with Pb^{2+}. The Ca^{2+} concentration was kept constant at 10 μM while the Pb^{2+} concentration was varied. The dashed vertical line marks the $[Pb^{2+}]/[Ca^{2+}]$ ratio of 0.3, at which approximately half of the protein is in the Pb^{2+}-bound form. For comparison, the inset shows the FRET spectra of the C2α–LUV system at zero metal ion concentration (black), 10 μM Ca^{2+} (blue), and 20 μM Pb^{2+} (green).

effect of Pb^{2+} on the interactions between C2α and PIP_2 embedded in lipid bilayers. This was accomplished using protein-to-membrane FRET experiments. The tryptophan residues of C2α served as a donor. Dansyl-PE, a fluorescent lipid that was incorporated into the LUVs, served as an acceptor. The LUVs consisted of POPC, POPS, bp-PIP_2, and dansyl-PE in a 61:30:2:7 molar ratio.

To provide the baseline for Pb^{2+} experiments, we first measured the protein-to-membrane FRET in the absence of metal ions. We determined that, in addition to our standard decalcification procedures applied to C2α and buffers, the LUV preparations had to be decalcified to eliminate submicromolar concentrations of contaminating Ca^{2+} that were sufficient to promote C2α–membrane association. The metal titration experiments shown in Figure 9A were conducted with decalcified lipids. In these experiments, we titrated the divalent metal ion into the mixture of C2α and LUVs containing 2% PIP_2 and monitored the increase in the intensity of the dansyl emission band at 505 nm. The Ca^{2+}-driven protein–membrane binding curve was fit with eq 3, which produced a $[Ca^{2+}]_{1/2}$ of 0.7 ± 0.1 μM and an H_{Ca} of 1.5 ± 0.1. This represents an ~7-fold decrease in $[Ca^{2+}]_{1/2}$ compared to that obtained for the membranes lacking PIP_2.

As in the case of Ca^{2+}, the addition of Pb^{2+} ions to the mixture of apo C2α and PIP_2-containing LUVs resulted in a systematic increase in the protein-to-membrane FRET, albeit with a lower overall FRET efficiency. Fitting the Pb^{2+}-driven membrane binding curve produced a $[Pb^{2+}]_{1/2}$ of 1.3 ± 0.1 μM and an H_{Pb} of 2.1 ± 0.1. This represents an ~5-fold increase in the apparent affinity of C2α for Pb^{2+} compared to that of the PtdSer-containing LUVs lacking PIP_2.[6] Overall, our results show that the ability of Pb^{2+} and Ca^{2+} to drive protein–membrane association is comparable, and that the presence of PIP_2 in the membrane increases the affinity of C2α for metal ions several-fold.

To characterize the competitive behavior of Pb^{2+} with respect to Ca^{2+}, we prepared the ternary C2α–Ca^{2+}–LUV complex by adjusting the final concentration of Ca^{2+} to 10 μM. We titrated the complex with Pb^{2+}, while monitoring the intensity of the dansyl emission band. A steady decrease in FRET efficiency was observed (Figure 9B) with an increasing Pb^{2+} concentration. Neither Pb^{2+} nor Ca^{2+} appreciably quenches the dansyl fluorescence, as shown in Figure S3 of the Supporting Information. Moreover, the maximal attainable FRET efficiency in the Pb^{2+}-driven membrane association experiments is typically ~40–60% of what can be attained in Ca^{2+}-driven experiments. This is illustrated in the inset of Figure 9B with the FRET spectra of metal-free (black), Pb^{2+}-containing

dx.doi.org/10.1021/bi201850h | Biochemistry 2012, 51, 3349–3360

(green), and Ca^{2+}-containing (blue) C2α–LUV systems. Given these properties of the C2α–LUV–metal ion system, we interpreted the decrease in FRET efficiency in the competition experiments as Pb^{2+} gradually displacing Ca^{2+} from the protein. A plateau region, indicative of full Ca^{2+} displacement by Pb^{2+}, is reached at a Pb:Ca ratio of 1.0.

The results of the reverse experiment, in which we attempted to outcompete Pb^{2+} with Ca^{2+}, are shown in Figure S4 of the Supporting Information. In agreement with our previous observations, we detected a steady increase in FRET efficiency with an increasing Ca^{2+} concentration, until it reached a plateau value at a Ca:Pb ratio of ~10. A comparison of the competition data demonstrates that Pb^{2+} is more effective than Ca^{2+} in displacing the competing metal ion from C2α in the presence of PIP_2-containing membranes. In vivo, the specifics of the Pb^{2+} versus Ca^{2+} competition behavior would depend on the relative and absolute bioavailable concentrations of these metal ions.

We have previously shown that, in addition to mediating the protein–membrane interactions, Pb^{2+} itself could associate with PtdSer-containing LUVs.[6] To test the influence of PIP_2 on this process, we combined vesicle sedimentation assays with inductively coupled plasma (ICP) detection of Pb^{2+} in the pellet and supernatant fractions. No protein was added to the samples. We explored two total lipid concentration regimes: 1.5 mM and 150 μM (as used in FRET experiments depicted in Figure 9). The results are summarized in Figures S5 and S6 of the Supporting Information. For comparison, we also included the data obtained in our previous work on the association of Pb^{2+} with vesicles lacking PIP_2.

The ICP data clearly demonstrate that the presence of PIP_2 in the LUVs increases the fractional population of the membrane-associated Pb^{2+}. This trend is especially prominent for the "high-lipid" regime of 1.5 mM, in which, depending on the total Pb^{2+} concentration, 60–90% of the total Pb^{2+} is membrane-associated. Under the conditions of our FRET experiments (150 μM total lipids and, e.g., 2.2 μM total Pb^{2+}), 76% of the Pb^{2+} is in the supernatant fraction for the PtdSer-containing vesicles lacking PIP_2; this value decreases to 33% in the presence of 2% PIP_2. This binding equilibrium effectively reduces the amount of Pb^{2+} available for C2α and would have an effect of overestimating the $[Pb^{2+}]_{1/2}$ value from the data shown in Figure 9A.

DISCUSSION

The experiments described here were designed to determine the influence of PIP_2 on the C2α–Pb^{2+} interactions, with the ultimate objective of gaining insight into the molecular mechanism of interference of Pb^{2+} with the Ca^{2+}-dependent function of C2 domains. There are three "checkpoints" where Pb^{2+} interference can occur: (1) interaction with the membrane-free C2 via the high-affinity Pb^{2+}-binding site(s) of the protein, (2) modulation of the metal-dependent C2–membrane association, and (3) direct interaction with the anionic membrane-binding sites. In our previous studies of the ternary system composed of C2α, Pb^{2+} ions, and PtdSer-containing LUVs, we determined that checkpoints 1 and possibly 3 are the most likely routes. Given the significant role of PIP_2 in C2α localization and membrane binding, we sought to determine the mutual effect of PIP_2 and Pb^{2+} on their respective interactions with C2α. Along with the Pb^{2+}-specific data, we obtained PIP_2 binding information for the apo and Ca^{2+}-complexed states of C2α. Taken together, this information allowed us to dissect the contribution of individual metal-binding sites to PIP_2 binding and evaluate the competitive behavior of Pb^{2+} with respect to Ca^{2+}.

Apo C2α Is a Low-Affinity PIP_2 Binding Module. Using NMR-detected titration of apo C2α with soluble C4-PIP_2, we identified protein regions whose electronic environment changed as a result of PIP_2 binding. The chemical shift perturbation data of Figure 3 show that this region is not limited to the lysine-rich cluster but also involves two calcium-binding loops (CBL1 and CBL3). The β-strands flanking CBL3, β6 and β7, are also affected by PIP_2. Superposition of the apo and ligand-bound C2α crystal structures revealed very few differences in the overall domain conformation, including the functional regions: the pairwise rmsd values for the backbone atoms do not exceed 0.5 Å (Figure S8 of the Supporting Information). This means that large chemical shift perturbations upon PIP_2 binding are most likely due to the changes in the electrostatic environment and/or conformational dynamics of the protein rather than changes in its average conformation.

The affinity of C2α for PIP_2 is rather weak (1.13 mM) in the absence of metal ions. The NMR-detected binding curves could be fit well with eq 2, indicating the presence of a single PIP_2-binding site on apo C2α. These data are in agreement with the results of previous studies on the GST-fused C2 domains[32] and the SPR study of the C2–membrane interactions.[38] The metal-independent association of C2α with PIP_2-containing membranes was not detectable under the conditions of our FRET experiments (Figure 9).

How prevalent are the metal ion-independent interactions with PIP_2 among the C2 domains? Both C2 domains of rabphilin-3A can interact with inositol 1,4,5-triphosphate, a headgroup of PIP_2, in a Ca^{2+}-independent manner.[37] Calcium-independent association with PIP_2-containing membranes was reported for the C2B domains of synaptotagmin 1[35,56] and synaptotagmin 9.[57] The physiological significance of the apo C2–PIP_2 interaction, as formulated for the C2B domain of synaptotagmin 1, is to increase the speed of the response of the host protein to Ca^{2+} by generating the protein state that is already prebound to the membrane.[35]

Progressive Saturation of Metal-Binding Sites Increases the Affinity of C2α for PIP_2. The 2000-fold difference in the affinities of C2α for $Pb^{2+}(1)$ and $Pb^{2+}(2)$ allowed us to prepare the state of C2α with the metal ion bound to site (1) only. This state, C2α·Pb, along with apo C2α and C2α·Ca_2, was used to determine the contribution of individual metal sites to PIP_2 binding. The equilibria of Figure 7 indicate that the affinity of C2α for PIP_2 increases several-fold upon progressive saturation of metal-binding sites. The K_d is reduced 6-fold for the C2α·Pb·PIP_2 complex compared to that of the C2α·PIP_2 complex, from 1.13 mM to 198 μM. The K_d is further reduced 8-fold for the C2α·Pb_2·PIP_2 complex compared to that of the C2α·Pb·PIP_2 complex, from 198 to 26 μM. Expressed in terms of free energies, the $\Delta(\Delta G^\circ)$ contributions of the first and second Pb^{2+} ions to the C2α–PIP_2 binding reactions are $-1.7RT$ and $-2.0RT$, respectively. We conclude that metal ions make individual and comparable contributions to the energetics of binding of PIP_2 to C2α.

The increase in the affinity of C2α for PIP_2 does not appear to depend on the nature of the metal ion. We reached this conclusion by comparing the dissociation constants of PIP_2 from the C2α·Pb_2·PIP_2 and C2α·Ca_2·PIP_2 complexes. The K_d values are similar for the Ca^{2+} and Pb^{2+} complexes (48 and 26 μM, respectively).

The ability of Ca^{2+}-dependent C2 domains to associate with anionic lipids and protein partners in response to binding Ca^{2+} has been attributed to the "electrostatic switch" mechanism.[3,12,13,58] The basic premise of this mechanism is that the binding of Ca^{2+} ions increases the electrostatic potential of C2 domains and hence improves its attraction to the negatively charged interacting partner. Figure 10 shows the calculated

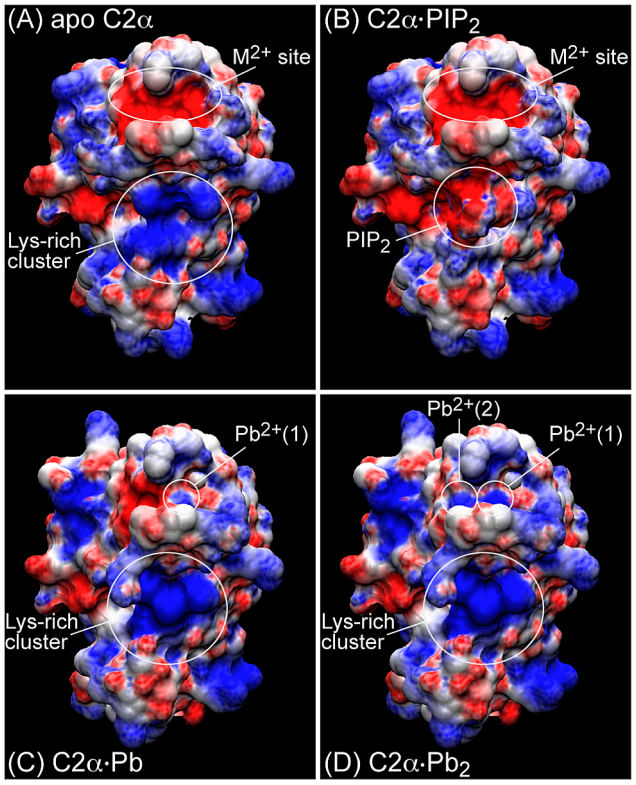

Figure 10. Electrostatic potential mapped onto the surface of (A) apo C2α, (B) C2α·PIP_2, (C) C2α·Pb, and (D) C2α·Pb_2. The color coding corresponds to the electrostatic potential ranging from $-6k_bT/e$ (red) to $6k_bT/e$ (blue). Structures in panels A and B were generated using PIP_2-bound C2α (PDB entry 3GPE), and structures in panels C and D were generated using Pb^{2+}-complexed C2α (PDB entry 3TWY).

electrostatic potential of C2α mapped onto the crystal structures. Apo C2α has a negatively charged metal-binding site formed by the aspartate residues and a positively charged lysine-rich cluster (panel A). The interaction of PIP_2 with the lysine-rich cluster results in a decrease in the electrostatic potential of the complex (panel B). In contrast, binding of Pb^{2+} (or Ca^{2+}) to C2α increases the electrostatic potential of the complex and improves its attraction to the negatively charged PIP_2. The individual contributions of Pb^{2+} ions are illustrated in panels C and D. Given that binding of metal to C2α does not appreciably change the conformational dynamics of the $\beta3-\beta4$ segment (Figure S9 of the Supporting Information), we conclude that the modulation of the affinity of C2α for PIP_2 by metal ions is mostly electrostatic in nature.

PIP_2 Increases the Affinity of C2α for Pb^{2+}. Prebound PIP_2 enhances the affinity of C2α for metal ions. In the presence of a saturating level of PIP_2, the affinity of C2α for $Pb^{2+}(1)$ increased 6-fold, from 67 to 12 nM. Similarly, the binding affinity of C2α for $Pb^{2+}(2)$ increased 8-fold, from 129 to 17 μM. Our data lend support to the TAMA ("target-activated messenger affinity") mechanism that was proposed by Falke's laboratory to explain how C2 domains, while being poor Ca^{2+} sensors in a membrane-free environment, are able to respond to micromolar concentrations of Ca^{2+} in the cell.[39] In the context of TAMA, membrane-embedded PIP_2 is the target and the metal ion is the messenger. The proximity (or prebinding) of C2α to PIP_2-containing membranes makes C2α more responsive to low concentrations of metal ions by increasing its binding affinity. This behavior has an immediate relevance to Pb^{2+} being a Ca^{2+} surrogate, because the presence of PIP_2 in the membranes will effectively sensitize C2α to the bioavailable concentrations of Pb^{2+}.

Pb^{2+} Facilitates the Association of C2α with PIP_2-Containing Lipid Membranes. We used protein-to-membrane FRET experiments to probe the Pb^{2+}-dependent association of C2α with the PIP_2-containing membranes. Similar to Ca^{2+}, we observed a steady increase in FRET efficiency as a function of metal ion concentration. In the Ca^{2+}-driven experiments, the incorporation of 2% PIP_2 into the membranes decreased $[Ca^{2+}]_{1/2}$ from 5 to 0.7 μM (~7-fold). Our data are in general agreement with the results of the previous SPR work[38] (4-fold decrease in Ca^{2+} K_d) and FRET studies with multicomponent mimics of the plasma membrane[39] (20-fold decrease in $[Ca^{2+}]_{1/2}$). In the Pb^{2+}-driven experiments, the incorporation of 2% PIP_2 into the membranes decreased $[Pb^{2+}]_{1/2}$ from 7 to 1.3 μM (~5-fold). This value is probably underestimated by a factor of ~2–3, because the sequestration of Pb^{2+} by the PIP_2- and PtdSer-containing membranes reduces the amount of Pb^{2+} available to C2α. Figures S5 and S6 of the Supporting Information illustrate how the presence of membrane-embedded PIP_2 enhances the interactions of Pb^{2+} with anionic membranes. In summary, the presence of PIP_2 in the membranes results in an enhancement of the affinity of C2α for divalent metal ions by roughly 1 order of magnitude.

Pb^{2+} Outcompetes Ca^{2+} in the Presence of Lipid Membranes. The ability of Pb^{2+} to compete with Ca^{2+} for protein-binding sites is what makes Pb^{2+} a potent environmental toxin. To assess the competitive behavior of Pb^{2+} in the context of C2α function, we conducted a Pb^{2+} versus Ca^{2+} competition experiment in the presence of PIP_2-containing membranes. As shown in Figure 9B, the displacement of Ca^{2+} from the ternary C2α–Ca^{2+}–LUV complex by Pb^{2+} can be readily monitored because of the differences in the maximal attainable FRET efficiency. Our data indicate that the equal population of Pb^{2+}- and Ca^{2+}-bound C2α species is reached at a $[Pb^{2+}]/[Ca^{2+}]$ ratio of 0.3. This corresponds to a Pb^{2+} concentration of 3.0 μM, which is ~2-fold lower than the value obtained in our previous experiments with the PtdSer-containing lipid membranes lacking PIP_2.[6]

Given the comparable ability of Pb^{2+} and Ca^{2+} to promote the association of C2α with lipid membranes, how does Pb^{2+} displace Ca^{2+}? We speculate that the displacement occurs through the interaction of Pb^{2+} with the high-affinity site on C2α (Figure 11). The Ca^{2+}-bound form of C2α exists in equilibrium between membrane-bound and membrane-free states (reaction 1). By itself, C2α is a low-affinity Ca^{2+} binding module, which makes the exact Ca^{2+} ligation state of membrane-free C2α difficult to ascertain. The interaction of Pb^{2+} with a single high-affinity site displaces Ca^{2+} from the protein (reaction 2), including the second metal-binding site. This occurs because saturating the high-affinity $Pb^{2+}(1)$ site on C2α decreases the affinity of the Ca^{2+} ion for the second site to

dx.doi.org/10.1021/bi201850h | Biochemistry 2012, 51, 3349–3360

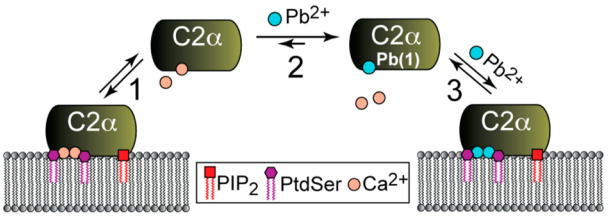

Figure 11. Pb^{2+} vs Ca^{2+} competition through the interaction with the C2α high-affinity metal-binding site.

~13 mM,[6] thereby precluding the formation of the mixed Pb^{2+}/Ca^{2+} species.

The concentrations of free Ca^{2+} in the cytosol are ~100 nM and 1 μM in the resting and stimulated states, respectively.[59] The concentration of bioavailable Pb^{2+} is in the picomolar to nanomolar range.[60] Given that the affinity of C2α for Pb^{2+}(1) exceeds its affinity for Ca^{2+} by more than 1000-fold, the formation of the C2α·Pb species in the cell is plausible.

The further fate of the C2α·Pb species depends on the bioavailable Pb^{2+} concentration. According to our FRET data, the high affinity of Pb^{2+}(1) for C2α does not translate into a high affinity of the C2α·Pb complex for the lipid membranes. The Hill coefficient of 2 that we obtained from the fit of the Pb^{2+}-driven FRET membrane binding curve implies that the binding of the second Pb^{2+} ion to C2α is required for protein–membrane association (reaction 3). The affinities of C2α for Pb^{2+}(2) and Ca^{2+} are comparable in the membrane-free form of the protein, which in turn results in the comparable ability of these two ions to drive C2α–membrane association (Figure 9A). If the concentration of Pb^{2+} in the cell is not sufficient to promote the association of C2α with membranes, Pb^{2+} binding may still activate PKCα by inducing the interdomain rearrangement within the regulatory domain of the enzyme. In either scenario, the presence of Pb^{2+}(1) at the high-affinity C2α site will interfere with the normal catalytic activity of PKCα by making the enzyme unresponsive to Ca^{2+} activation during the signaling event.

As a final note, the saturation of one Pb^{2+} site is not sufficient for C2α to undergo membrane association under the conditions used here. However, given the proposed mechanistic roles of individual Ca^{2+} sites[39] and our NMR results for binding of PIP_2 to the C2α·Pb complex, we cannot completely exclude the possibility that, at high local concentrations of anionic lipids, such as PtdSer and PIP_2, the association of C2α·Pb with membranes may in fact occur. This situation can arise upon the interaction of PKCα with its substrates, such as MARCKS (myristoylated alanine-rich C kinase substrate), that laterally sequesters PIP_2 molecules[61] and releases them upon phosphorylation by PKC or interactions with calmodulin.

CONCLUSIONS

Based on our results, we conclude that PIP_2 can influence two aspects of C2α–Pb^{2+}–membrane interactions: the affinity of C2α for Pb^{2+} and the association of Pb^{2+} with the anionic sites on the membrane. Both factors may play a role in the aberrant activation of PKCα and thus contribute to the toxic effect of Pb^{2+}. Divalent metal ions and PIP_2 enhance each other's affinity for C2α primarily through modulation of the protein's electrostatic properties. This behavior, which is independent of the nature of the divalent metal ion, demonstrates the synergy between two cofactors that are required for C2α function.

ASSOCIATED CONTENT

Supporting Information

Full NMR spectra of C2α in three states of metal ligation at varying concentrations of C4-PIP_2, fluorescence control experiments and Ca^{2+} versus Pb^{2+} competition results, ICP measurements of membrane-bound Pb^{2+}, cryoelectron microscopy images of LUV suspensions, superposition of C2α structures, Hahn–Echo relaxation data, and estimation of affinities of C2α for metal ions. This material is available free of charge via the Internet at http://pubs.acs.org.

AUTHOR INFORMATION

Corresponding Author

*Phone: (979) 845-6312. Fax: (979) 845-4946. E-mail: tigumenova@tamu.edu.

Funding

This work was supported by startup funds from Texas A&M University, a Ralph E. Powe junior faculty enhancement award from Oak Ridge Associated Universities (T.I.I.), and National Institutes of Health Training Grant 2-T32GM008523-13 (K.A.M.).

Notes

The authors declare no competing financial interest.

ACKNOWLEDGMENTS

We thank Prof. Donald W. Pettigrew (Texas A&M University) for access to the spectrofluorometer, Dr. Robert Taylor (Trace Element Research Laboratory, College of Veterinary Medicine, Texas A&M University) for conducting the ICP analysis, and Dr. Zhiping Luo (Microscopy and Imaging Center, Texas A&M University) for the cryoelectron microscopy measurements.

REFERENCES

(1) Cho, W., and Stahelin, R. V. (2006) Membrane binding and subcellular targeting of C2 domains. *Biochim. Biophys. Acta 1761*, 838–849.

(2) Nalefski, E. A., and Falke, J. J. (1996) The C2 domain calcium-binding motif: Structural and functional diversity. *Protein Sci. 5*, 2375–2390.

(3) Rizo, J., and Sudhof, T. C. (1998) C2-domains, structure and function of a universal Ca^{2+}-binding domain. *J. Biol. Chem. 273*, 15879–15882.

(4) Corbalán-García, S., and Gómez-Fernández, J. C. (2010) The C2 domains of classical and novel PKCs as versatile decoders of membrane signals. *Biofactors 36*, 1–7.

(5) Kohout, S. C., Corbalán-García, S., Torrecillas, A., Gómez-Fernández, J. C., and Falke, J. J. (2002) C2 domains of protein kinase C isoforms α, β, and γ: Activation parameters and calcium stoichiometries of the membrane-bound state. *Biochemistry 41*, 11411–11424.

(6) Morales, K. A., Lasagna, M., Gribenko, A. V., Yoon, Y., Reinhart, G. D., Lee, J. C., Cho, W., Li, P., and Igumenova, T. I. (2011) Pb^{2+} as modulator of protein-membrane interactions. *J. Am. Chem. Soc. 133*, 10599–10611.

(7) Ubach, J., Zhang, X. Y., Shao, X. G., Sudhof, T. C., and Rizo, J. (1998) Ca^{2+} binding to synaptotagmin: How many Ca^{2+} ions bind to the tip of a C-2-domain? *EMBO J. 17*, 3921–3930.

(8) Fernandez, I., Arac, D., Ubach, J., Gerber, S. H., Shin, O. H., Gao, Y., Anderson, R. G. W., Sudhof, T. C., and Rizo, J. (2001) Three-dimensional structure of the synaptotagmin 1 C2B-domain: Synaptotagmin 1 as a phospholipid binding machine. *Neuron 32*, 1057–1069.

(9) Stahelin, R. V., Rafter, J. D., Das, S., and Cho, W. (2003) The molecular basis of differential subcellular localization of C2 domains of

protein kinase C-α and group IVa cytosolic phospholipase A(2). *J. Biol. Chem. 278*, 12452−12460.
(10) Lomasney, J. W., Cheng, H. F., Roffler, S. R., and King, K. (1999) Activation of phospholipase Cδ1 through C2 domain by a Ca^{2+}-enzyme-phosphatidylserine ternary complex. *J. Biol. Chem. 274*, 21995−22001.
(11) Ananthanarayanan, B., Das, S., Rhee, S. G., Murray, D., and Cho, W. (2002) Membrane targeting of C2 domains of phospholipase C-δ isoforms. *J. Biol. Chem. 277*, 3568−3575.
(12) Zhang, X., Rizo, J., and Sudhof, T. C. (1998) Mechanism of phospholipid binding by the C2A-domain of synaptotagmin I. *Biochemistry 37*, 12395−12403.
(13) Murray, D., and Honig, B. (2002) Electrostatic control of the membrane targeting of C2 domains. *Mol. Cell 9*, 145−154.
(14) Shao, X. G., Fernandez, I., Sudhof, T. C., and Rizo, J. (1998) Solution structures of the Ca^{2+}-free and Ca^{2+}-bound C(2)A domain of synaptotagmin I: Does Ca^{2+} induce a conformational change? *Biochemistry 37*, 16106−16115.
(15) Verdaguer, N., Corbalán-García, S., Ochoa, W. F., Fita, I., and Gómez-Fernández, J. C. (1999) Ca^{2+} bridges the C2 membrane-binding domain of protein kinase Cα directly to phosphatidylserine. *EMBO J. 18*, 6329−6338.
(16) Stahelin, R. V., Wang, J. Y., Blatner, N. R., Raftner, J. D., Murray, D., and Cho, W. H. (2005) The origin of C1A-C2 interdomain interactions in protein kinase Cα. *J. Biol. Chem. 280*, 36452−36463.
(17) Vrljic, M., Strop, P., Ernst, J. A., Sutton, R. B., Chu, S., and Brunger, A. T. (2010) Molecular mechanism of the synaptotagmin-SNARE interaction in Ca^{2+}-triggered vesicle fusion. *Nat. Struct. Mol. Biol. 17*, 325−331.
(18) Godwin, H. A. (2001) The biological chemistry of lead. *Curr. Opin. Chem. Biol. 5*, 223−227.
(19) Suszkiw, J. B. (2004) Presynaptic disruption of transmitter release by lead. *Neurotoxicology 25*, 599−604.
(20) Bouton, C. M., Frelin, L. P., Forde, C. E., Arnold Godwin, H., and Pevsner, J. (2001) Synaptotagmin I is a molecular target for lead. *J. Neurochem. 76*, 1724−1735.
(21) Newton, A. C. (2001) Protein kinase C: Structural and spatial regulation by phosphorylation, cofactors, and macromolecular interactions. *Chem. Rev. 101*, 2353−2364.
(22) Steinberg, S. F. (2008) Structural basis of protein kinase C isoform function. *Physiol. Rev. 88*, 1341−1378.
(23) Majewski, H., and Iannazzo, L. (1998) Protein kinase C: A physiological mediator of enhanced transmitter output. *Prog. Neurobiol. 55*, 463−475.
(24) Stevens, C. F., and Sullivan, J. M. (1998) Regulation of the readily releasable vesicle pool by protein kinase C. *Neuron 21*, 885−893.
(25) Markovac, J., and Goldstein, G. W. (1988) Picomolar concentrations of lead stimulate brain protein kinase C. *Nature 334*, 71−73.
(26) Tomsig, J. L., and Suszkiw, J. B. (1995) Multisite interactions between Pb^{2+} and protein kinase C and its role in norepinephrine release from bovine adrenal chromaffin cells. *J. Neurochem. 64*, 2667−2673.
(27) Long, G. J., Rosen, J. F., and Schanne, F. A. (1994) Lead activation of protein kinase C from rat brain. Determination of free calcium, lead, and zinc by ^{19}F NMR. *J. Biol. Chem. 269*, 834−837.
(28) Sun, X. Y., Tian, X. T., Tomsig, J. L., and Suszkiw, J. B. (1999) Analysis of differential effects of Pb^{2+} on protein kinase C isozymes. *Toxicol. Appl. Pharmacol. 156*, 40−45.
(29) Di Paolo, G., and De Camilli, P. (2006) Phosphoinositides in cell regulation and membrane dynamics. *Nature 443*, 651−657.
(30) McLaughlin, S., and Murray, D. (2005) Plasma membrane phosphoinositide organization by protein electrostatics. *Nature 438*, 605−611.
(31) Di Paolo, G., Moskowitz, H. S., Gipson, K., Wenk, M. R., Voronov, S., Obayashi, M., Flavell, R., Fitzsimonds, R. M., Ryan, T. A., and De Camilli, P. (2004) Impaired PtdIns(4,5)P2 synthesis in nerve terminals produces defects in synaptic vesicle trafficking. *Nature 431*, 415−422.
(32) Corbalán-García, S., García-García, J., Rodriguez-Alfaro, J. A., and Gómez-Fernández, J. C. (2003) A new phosphatidylinositol 4,5-bisphosphate-binding site located in the C2 domain of protein kinase Cα. *J. Biol. Chem. 278*, 4972−4980.
(33) Guerrero-Valero, M., Marin-Vicente, C., Gómez-Fernández, J. C., and Corbalán-García, S. (2007) The C2 domains of classical PKCs are specific PtdIns(4,5)P2-sensing domains with different affinities for membrane binding. *J. Mol. Biol. 371*, 608−621.
(34) Schiavo, G., Gu, Q. M., Prestwich, G. D., Sollner, T. H., and Rothman, J. E. (1996) Calcium-dependent switching of the specificity of phosphoinositide binding to synaptotagmin. *Proc. Natl. Acad. Sci. U.S.A. 93*, 13327−13332.
(35) Bai, J., Tucker, W. C., and Chapman, E. R. (2004) PIP_2 increases the speed of response of synaptotagmin and steers its membrane-penetration activity toward the plasma membrane. *Nat. Struct. Mol. Biol. 11*, 36−44.
(36) Coudevylle, N., Montaville, P., Leonov, A., Zweckstetter, M., and Becker, S. (2008) Structural determinants for Ca^{2+} and phosphatidylinositol 4,5-bisphosphate binding by the C2A domain of rabphilin-3A. *J. Biol. Chem. 283*, 35918−35928.
(37) Montaville, P., Coudevylle, N., Radhakrishnan, A., Leonov, A., Zweckstetter, M., and Becker, S. (2008) The PIP_2 binding mode of the C2 domains of rabphilin-3A. *Protein Sci. 17*, 1025−1034.
(38) Manna, D., Bhardwaj, N., Vora, M. S., Stahelin, R. V., Lu, H., and Cho, W. (2008) Differential roles of phosphatidylserine, PtdIns(4,5)P2, and PtdIns(3,4,5)P3 in plasma membrane targeting of C2 domains. Molecular dynamics simulation, membrane binding, and cell translocation studies of the PKCα C2 domain. *J. Biol. Chem. 283*, 26047−26058.
(39) Corbin, J. A., Evans, J. H., Landgraf, K. E., and Falke, J. J. (2007) Mechanism of specific membrane targeting by C2 domains: Localized pools of target lipids enhance Ca^{2+} affinity. *Biochemistry 46*, 4322−4336.
(40) Radhakrishnan, A., Stein, A., Jahn, R., and Fasshauer, D. (2009) The Ca^{2+} affinity of synaptotagmin 1 is markedly increased by a specific interaction of its C2B domain with phosphatidylinositol 4,5-bisphosphate. *J. Biol. Chem. 284*, 25749−25760.
(41) Evans, J. H., Murray, D., Leslie, C. C., and Falke, J. J. (2006) Specific translocation of protein kinase Cα to the plasma membrane requires both Ca^{2+} and PIP_2 recognition by its C2 domain. *Mol. Biol. Cell 17*, 56−66.
(42) Sanchez-Bautista, S., Marin-Vicente, C., Gómez-Fernández, J. C., and Corbalán-García, S. (2006) The C2 domain of PKCα is a Ca^{2+}-dependent PtdIns(4,5)P2 sensing domain: A new insight into an old pathway. *J. Mol. Biol. 362*, 901−914.
(43) Guerrero-Valero, M., Ferrer-Orta, C., Querol-Audi, J., Marin-Vicente, C., Fita, I., Gómez-Fernández, J. C., Verdaguer, N., and Corbalán-García, S. (2009) Structural and mechanistic insights into the association of PKCα-C2 domain to PtdIns(4,5)P2. *Proc. Natl. Acad. Sci. U.S.A. 106*, 6603−6607.
(44) Kohout, S. C., Corbalán-García, S., Gómez-Fernández, J. C., and Falke, J. J. (2003) C2 domain of protein kinase Cα: Elucidation of the membrane docking surface by site-directed fluorescence and spin labeling. *Biochemistry 42*, 1254−1265.
(45) Marley, J., Lu, M., and Bracken, C. (2001) A method for efficient isotopic labeling of recombinant proteins. *J. Biomol. NMR 20*, 71−75.
(46) Barenholz, Y., and Amselem, S. (1993) *Liposome Technology*, 2nd ed., Vol. *1*, CRC Press, Boca Raton, FL.
(47) Delaglio, F., Grzesiek, S., Vuister, G. W., Zhu, G., Pfeifer, J., and Bax, A. (1995) NMRPipe: A multidimensional spectral processing system based on Unix pipes. *J. Biomol. NMR 6*, 277−293.
(48) Goddard, T. D., and Kneller, D. G. (2008) *SPARKY 3*, University of California, San Francisco.
(49) Schumann, F. H., Riepl, H., Maurer, T., Gronwald, W., Neidig, K. P., and Kalbitzer, H. R. (2007) Combined chemical shift changes

and amino acid specific chemical shift mapping of protein-protein interactions. *J. Biomol. NMR 39*, 275−289.
(50) Wilcox, C. S. (1991) Design, synthesis, and evaluation of an efficacious functional group dyad. Methods and limitations in the use of NMR for measuring host-guest interactions. In *Frontiers in Supramolecular Organic Chemistry and Photochemistry* (Schneider, H. J., and Dürr, H., Eds.) pp 123−143, Wiley-VCH, Weinheim, Germany.
(51) Baker, N. A., Sept, D., Joseph, S., Holst, M. J., and McCammon, J. A. (2001) Electrostatics of nanosystems: Application to microtubules and the ribosome. *Proc. Natl. Acad. Sci. U.S.A. 98*, 10037−10041.
(52) Humphrey, W., Dalke, A., and Schulten, K. (1996) VMD: Visual molecular dynamics. *J. Mol. Graphics 14*, 27−38.
(53) Dolinsky, T. J., Czodrowski, P., Li, H., Nielsen, J. E., Jensen, J. H., Klebe, G., and Baker, N. A. (2007) PDB2PQR: Expanding and upgrading automated preparation of biomolecular structures for molecular simulations. *Nucleic Acids Res. 35*, W522−W525.
(54) McLaughlin, S., Wang, J., Gambhir, A., and Murray, D. (2002) PIP(2) and proteins: Interactions, organization, and information flow. *Annu. Rev. Biophys. Biomol. Struct. 31*, 151−175.
(55) Kazantsev, A. V., Krivenko, A. A., and Pace, N. R. (2009) Mapping metal-binding sites in the catalytic domain of bacterial RNase P RNA. *RNA 15*, 266−276.
(56) Kuo, W. W., Herrick, D. Z., and Cafiso, D. S. (2011) Phosphatidylinositol 4,5-bisphosphate alters synaptotagmin 1 membrane docking and drives opposing bilayers closer together. *Biochemistry 50*, 2633−2641.
(57) Tucker, W. C., Edwardson, J. M., Bai, J., Kim, H. J., Martin, T. F., and Chapman, E. R. (2003) Identification of synaptotagmin effectors via acute inhibition of secretion from cracked PC12 cells. *J. Cell Biol. 162*, 199−209.
(58) Shao, X., Li, C., Fernández, I., Zhang, X., Sudhof, T. C., and Rizo, J. (1997) Synaptotagmin-syntaxin interaction: The C2 domain as a Ca^{2+}-dependent electrostatic switch. *Neuron 18*, 133−142.
(59) Parekh, A. B. (2011) Decoding cytosolic Ca^{2+} oscillations. *Trends Biochem. Sci. 36*, 78−87.
(60) Claudio, E. S., Godwin, H. A., and Magyar, J. S. (2003) Fundamental coordination chemistry, environmental chemistry, and biochemistry of lead(II). *Prog. Inorg. Chem. 51*, 1−144.
(61) Gambhir, A., Hangyas-Mihalyne, G., Zaitseva, I., Cafiso, D. S., Wang, J., Murray, D., Pentyala, S. N., Smith, S. O., and McLaughlin, S. (2004) Electrostatic sequestration of PIP_2 on phospholipid membranes by basic/aromatic regions of proteins. *Biophys. J. 86*, 2188−2207.